Applied Catalysis B: Environmental 104 (2011) 382–389

Contents lists available at ScienceDirect

Applied Catalysis B: Environmental

journal homepage: www.elsevier.com/locate/apcatb

Electrocatalytic activity of Pt nanoparticles on a karst-like Ni thin film toward methanol oxidation in alkaline solutions

Chung-Shou Chen, Fu-Ming Pan*, Hsin-Jung Yu

Department of Materials Science and Engineering, National Chiao-Tung University, 1001 Ta Hsueh Road, Hsinchu 30010, Taiwan, ROC

ARTICLE INFO

Article history:
Received 1 December 2010
Received in revised form 18 February 2011
Accepted 3 March 2011
Available online 10 March 2011

Keywords:
Nickel
Platinum nanoparticles
DMFC
CO tolerance
Alkaline solution

ABSTRACT

The study prepared rugged Ni thin films for the study on electrocatalytic methanol oxidation reaction (MOR) in alkaline solutions. The rugged Ni thin film has a karst-like morphology, which provides a large surface area for Pt nanoparticle loading by pulse electrodeposition. Cyclic voltammetry measurements showed that the Pt/karst-Ni electrode had a high electrocatalytic activity toward MOR and CO tolerance in the KOH electrolyte. $Ni(OH)_2$ formed on the Ni support during the potential scan can enhance CO tolerance of Pt nanoparticles via the bi-functional mechanism. The Langmuir–Hinshelwood and the Eley–Rideal mechanisms are used to elucidate the role of OH surface groups on the Ni support and OH^- ions in the electrolyte, respectively, in the enhancement of the CO tolerance. XPS analysis indicates that negative charges transfer from the Ni support to Pt nanoparticles. The electronic interaction may modify adsorption properties of CO adspecies on the Pt catalyst; the modification allows easy CO electro-oxidation by OH species surrounding the Pt nanoparticles, either from the Ni support or from the alkaline solution. The synergistic effect of the bifunctional mechanism and the electronic interaction makes the Pt/karst-Ni structure a good catalytic electrode for MOR in the KOH solution.

1. Introduction

Direct methanol fuel cells (DMFCs) are very attractive for mobile power source applications, such as automotive systems and portable electronics, because they are lightweight, power-efficient and with a long use-life. Although extensive study on DMFCs has been being carried out for several decades, practical commercialization of DMFCs still faces many challenges associated with materials and technical shortcomings, including high cost of Pt-based electrocatalysts, low electroactivity of methanol oxidation reaction (MOR), poor kinetics of oxygen reduction reaction (ORR), and methanol crossover [1,2]. Among various attempts to improve electrochemical performance of DMFCs, the study on the improvement in the electrocatalytic activity of Pt toward MOR receives the most attention. One major approach to improving the MOR electroactivity is to increase the resistance of Pt catalysts against CO poisoning, which results from catalytic site blocking by carbonaceous byproducts due to incomplete methanol oxidation [1,3,4]. The CO poisoning effect can be alleviated by the so called bi-functional mechanism, which governs the electro-oxidation reaction of the carbonaceous byproducts with neighboring OH adspecies. A fast removal rate of the carbonaceous adspecies can continuously create free adsorption sites for methanol molecules, thus resulting in a high reaction rate of methanol electro-oxidation. Pt-based binary and ternary alloys have shown an enhanced electrocatalytic activity toward MOR because of better CO tolerance of Pt in the alloys. [1,4–7] Many transition metals, such as Sn, Ni and Co, [8–10] and metal oxides, such as CeO_2, SnO_2, RuO_2, WO_X and TiO_2, are also used as a promoter or the Pt catalyst support to improve CO tolerance [11–16]. Pt is known to have a higher CO tolerance in alkaline media than in acidic media, and thus exhibit better electrocatalytic performance for methanol oxidation in alkaline electrolytes [6,17]. The better CO tolerance in alkaline media is generally ascribed to the abundance of OH^- ions in the electrolyte, which can effectively oxidize carbonaceous adspecies on the Pt catalyst via the Eley–Rideal mechanism [18,19]. Because the electrocatalytic activity of Pt toward MOR can be readily improved by using alkaline electrolytes, direct methanol alkali fuel cells (DMAFCs), which is an alkali analogue of DMFCs, have recently received much interest. Besides, compared with DMFCs, DMAFCs have a faster oxygen reduction kinetics [1,20] and less methanol crossover [21].

Transition metals are generally very corrosion resistant in alkaline solutions, and therefore they are good electrode materials for DMAFC applications. Because nickel hydroxides formed on Ni surfaces may act as chemical oxidizing agents for methanol oxidation in alkaline solutions [22,23], the addition of Ni in Pt/Ru alloys can enhance the electrocatalytic activity of the electrode toward MOR [4]. Nickel has also been used as the Pt catalyst support for methanol

* Corresponding author. Tel.: +886 3 5131322; fax: +886 3 5724727.
E-mail address: fmpan@faculty.nctu.edu.tw (F.-M. Pan).

0926-3373/$ – see front matter © 2011 Elsevier B.V. All rights reserved.
doi:10.1016/j.apcatb.2011.03.002

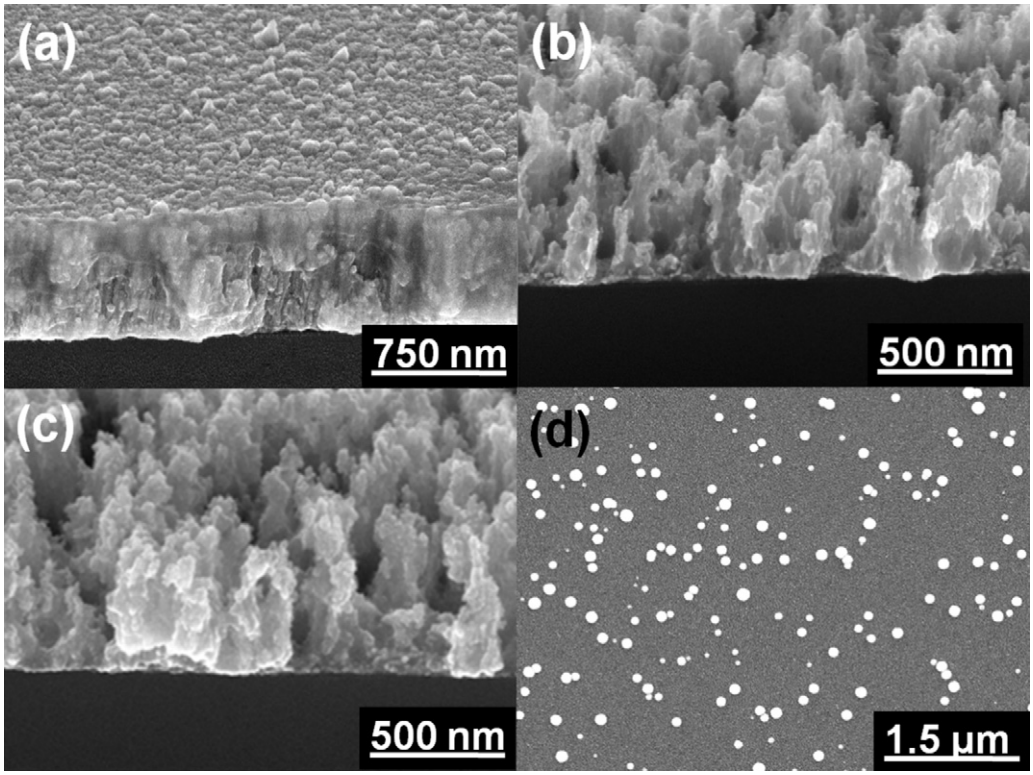

Fig. 1. SEM images of (a) the as-deposited metallic nickel thin film, (b) the as-prepared karst-Ni thin film, (c) the karst-Ni thin film after the pulse-electrodeposition of Pt nanoparticles, and (d) the blanket-Ni thin film with pulse-electrodeposited Pt particles.

electro-oxidation in alkaline solutions to enhance CO tolerance [1,23]. In this study, we used HNO_3 wet-etch to prepare rugged Ni thin films, on which Pt nanoparticles were pulse-electrodeposited, for the study of electrocatalytic methanol oxidation in alkaline solutions. The rugged Ni thin film has a karst-like morphology, and is referred to as karst-Ni thin film thereafter. Pt nanoparticles on the karst-Ni thin film demonstrate a great improvement in the electrocatalytic performance for methanol oxidation in the alkaline electrolyte as compared with a blanket Pt thin film and Pt particles on a blanket Ni thin film.

2. Experimental

To prepare the karst-Ni support, a 10 nm thick Ti thin film and a 700 nm thick Ni thin film were sequentially deposited on a 6-in. p-type Si(1 0 0) wafer of low resistivity (0.002 Ω-cm) by electron beam evaporation (e-beam) deposition. The Ti thin film was used as the adhesion layer for the Ni thin film. The Ni/Ti film was immersed in an aqueous solution of 8% hydrofluoric acid at 30 °C for 3 min to remove the surface nickel oxide, followed by a rinse with deionized (DI) water. The wet-cleaned thin film was then etched by an aqueous solution of 0.05 M HNO_3 to produce a rugged surface on the Ni thin film. Before the pulse electrodeposition of Pt nanoparticles, the rugged Ni thin film received sequentially a rinse of DI water and a N_2 purge.

Pt nanoparticles were electrodeposited on the karst-Ni support in a mixed aqueous solution of 0.001 M H_2PtCl_6 and 0.06 M HCl at room temperature by galvanostatic pulse plating in a two-electrode cell system. The karst-Ni support was used as the working electrode and a Pt disk (1.5 cm in diameter) as the counter electrode. During the pulse electrodeposition, the square wave pulsed current was switched between −1.0 and 0 mA, and both the anodic and cathodic pulse durations were 1 ms. A total of 800 pulse cycles were performed to deposit Pt nanoparticles on the karst-Ni support. For comparison, we also pulse-electrodeposited Pt particles on a blanket Ni thin film without the HNO_3 wet etch (denoted as Pt/Ni thereafter), and prepared a 5 nm thick Pt thin film on the Ti thin film capped Si wafer by e-beam deposition. For the preparation of the Pt/Ni electrode, following Pt electrodeposition conditions were used: the pulse current: −1.0 to 0 mA, the anodic and cathodic pulse durations: 100 ms, and the pulse cycle number: 200. The mass loading of the Pt electrocatalyst on the support was determined by inductively coupled plasma mass spectroscopy (ICP-MS, Thermo X Series II), and was used to calculate the electrochemical surface active area (ESA) and the mass activity of the Pt catalyst. The Pt mass loadings of the Pt/karst Ni, the Pt/Ni and the Pt thin film electrodes discussed in the work are 0.064, 0.034 and 0.031 mg/cm^2, respectively.

Electrochemical measurements were performed at room temperatures in a three electrode cell system with a saturated calomel reference electrode (SCE). The Ni supported Pt electrode was used as the working electrode and a Pt disk as the counter electrode. All aqueous solutions were prepared with low resistance DI water (∼18 ΩM). The cyclic voltammetry measurement of methanol electro-oxidation was conducted in a deaerated solution of 1 M KOH and 1 M CH_3OH within the potential range from −0.9 to 0.2 V vs. SCE with a scan rate of 20 mV s^{-1}. The CO stripping measurement was carried out in a 1 M KOH solution within the potential range from −1.04 to 0.4 V with a scan rate of 20 mV s^{-1}. A monolayer of CO was adsorbed on the Pt/Ni catalyst by flowing a 10% CO/N_2 gas mixture in the 1 M KOH aqueous solution at −1.04 V for 30 min. The chronoamperometric measurement for methanol oxidation was carried out in the solution of 1 M KOH + 1 M CH_3OH at −0.3 V for 3600 s.

Surface morphology was studied by scanning electron microscopy (SEM, JEOL JSM-6500F). The crystallinity and the chemical composition of electrode samples were examined by x-ray diffractometry (XRD, PANalytical X'Pert Pro) with the Cu Kα source and x-ray photoelectron spectroscopy (XPS, Thermo VG 350), respectively. To calibrate the binding energy of photo-

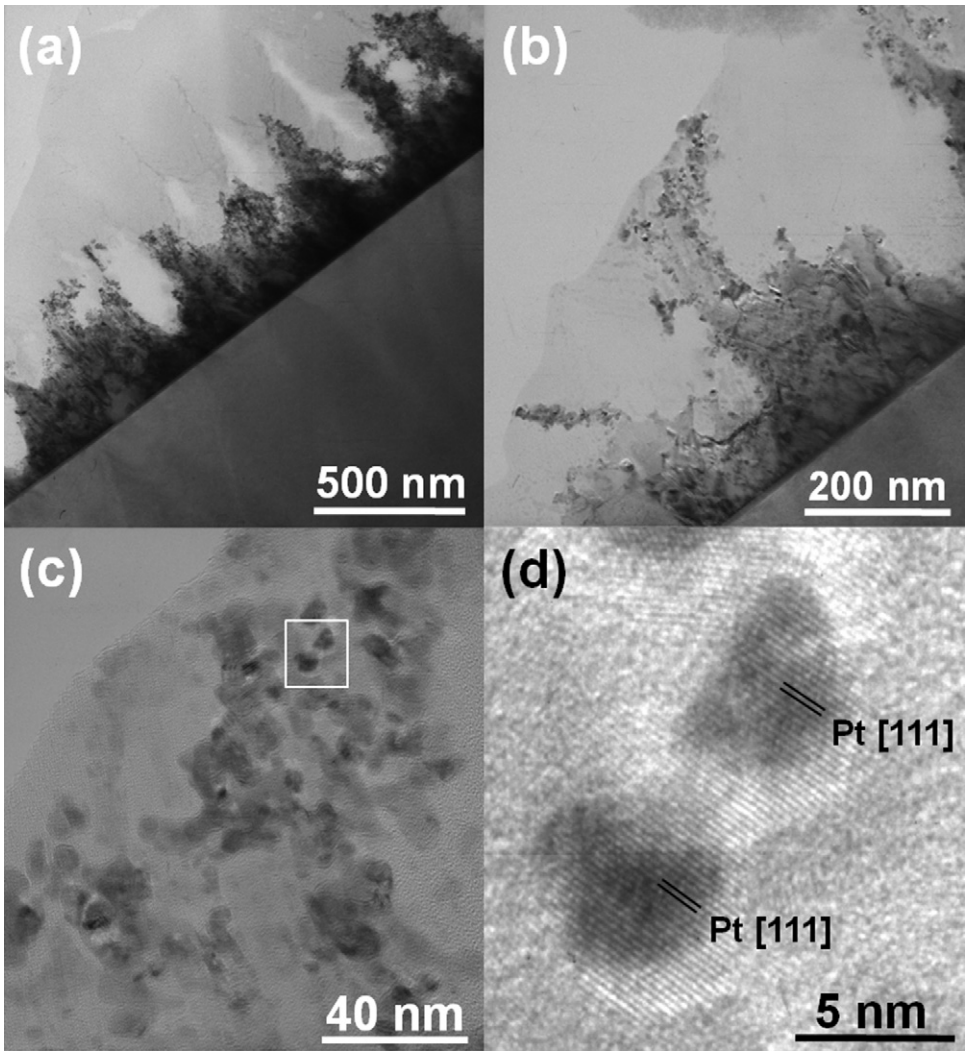

Fig. 2. TEM images of the karst-Ni thin film with electrodeposited Pt nanoparticles in different magnifications (a), (b) and (c); HRTEM image of Pt nanoparticles on the karst-Ni support (d).

electrons emitted from bare nickel oxide samples, we deposited an ultrathin Pt film (<3 nm) on the sample surface by e-beam evaporation and used the Pt $4f_{7/2}$ peak as the reference. For the binding energy calibration for Pt loaded samples, an ultrathin Au film was deposited on the sample by thermal evaporation and the Au $4f_{7/2}$ peak was used as the reference. The microstructure of the karst-Ni thin film and Pt nanoparticles was studied by transmission electron microscopy (TEM, Philips tacnai 20). To protect the rugged surface of the karst-Ni thin film from being damaged during TEM specimen preparation, a 400 nm thick SiO_2 overlayer was deposited on the film surface by high density plasma chemical vapor deposition.

3. Results and discussion

3.1. Material characterizations

The e-beam deposited Ni thin film becomes very rugged after the HNO_3 wet etch, and has a surface morphology like a karst landform; we thus refer to the rugged Ni thin film as the karst-Ni thin film. The surface of the karst-Ni thin film is full of protruding structures of irregular shapes and cavities as shown in the cross-sectional SEM image of Fig. 1(b). To illustrate the dramatic change in the surface morphology of the Ni thin film after the HNO_3 wet etch, the as-deposited Ni thin film is shown in Fig. 1(a). The open and rugged surface of the karst-Ni thin film provides a large loading area for electrodeposited Pt nanoparticles. Fig. 1(c) shows the side-view SEM image of the karst-Ni thin film after the Pt pulse-electrodeposition (thereafter referred to as Pt/karst-Ni). The karst-Ni thin film retains its rugged morphology after the Pt electrodeposition, but the edge of the protruding structures becomes less sharp because of the accumulation of Pt nanoparticles. The size of the Pt nanoparticles is too small to be clearly observed in the SEM image. According to TEM analysis discussed later, the size of the Pt nanoparticles is about 5 nm in diameter. We also prepared a blanket Ni thin film, on which Pt particles were subsequently electrodeposited (referred to as Pt/Ni), and a blanket Pt thin film for comparison with the Pt/karst-Ni thin film on the electrocatalytic activity toward MOR. Fig. 1(d) shows an SEM image of the Pt/Ni thin film. Pt particles on the Pt/Ni thin film have a broad size distribution ranging from a few nm to hundreds of nanometers.

Fig. 2(a) shows a cross-sectional TEM image of the Pt/karst-Ni thin film. The irregularly shaped Ni nanostructures are decorated by dark spots of nanometer scale, which randomly distribute over the karst-Ni thin film as shown in the enlarged TEM image of Fig. 2(b) and (c). The Ni nanostructures exhibit a slightly porous feature as indicated by some areas of bright contrast. Fig. 2(d) shows a high resolution TEM image of two nanoparticles selected from the area marked by the square in the TEM image of Fig. 2(c). The lattice fringes clearly indicate that the nanoparticles are crystalline Pt

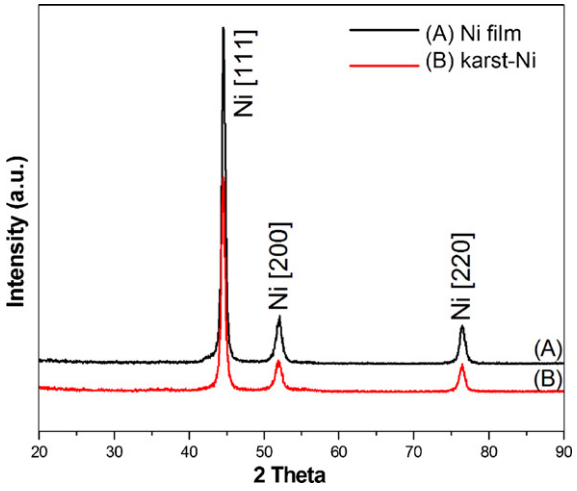

Fig. 3. X-ray diffraction spectra of the as-deposited Ni thin film and the karst-Ni thin film.

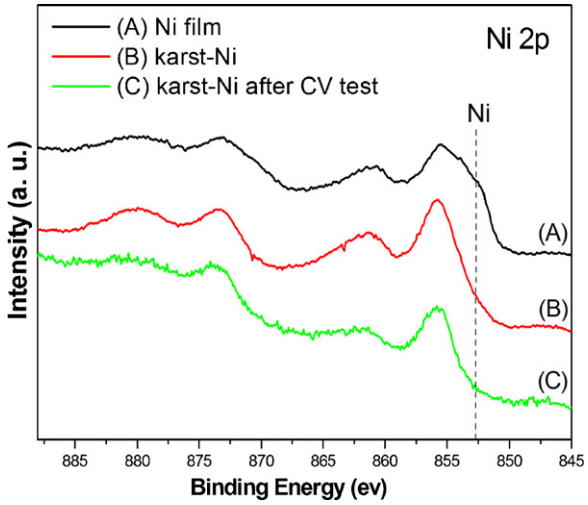

Fig. 4. Ni(2p) XPS spectra of the as-deposited Ni thin film, the as-prepared karst-Ni thin film and a karst-Ni thin film after a 10-cycle CV scan in the aqueous solution of 1 M CH_3OH + 1 M KOH. The dashed line marks the Ni $2p_{3/2}$ binding energy of metallic Ni.

grains with a diameter of ~5 nm. XRD analysis gives an average particle size slightly larger than 5 nm. Based on the peak width of the Pt(1 1 1) diffraction peak (not shown), the average particle size of Pt nanoparticles on the karst-Ni support is about 5.6 nm according to the Scherrer equation.

Many studies have shown that transition metal oxide supports can greatly enhance the electrocatalytic activity of Pt toward methanol oxidation [12,15]. The enhancement is generally ascribed to the bifunctional mechanism and/or the electronic effect, which are closely related to surface properties of the catalyst support [24–26]. To understand the surface property of the karst-Ni thin film, we used XRD and XPS to characterize chemical phases present on the HNO_3-etched Ni nanostructures. As shown in Fig. 3, the karst-Ni thin film has the same x-ray diffraction feature as the as-deposited blanket Ni thin film; the three diffraction peaks situated at 45°, 52° and 76° are due to the (1 1 1), (2 0 0) and (2 2 0) lattice planes, respectively, of the face centered cubic (FCC) lattice structure of metallic nickel. Although the XRD result suggests that the karst-Ni thin film is composed of metallic Ni, the XPS analysis shows that little metallic Ni is present on the surface of the karst-Ni thin film. The XPS spectra of the as-deposited Ni thin film and the karst-Ni thin film are shown in Fig. 4. The as-deposited blanket Ni thin film has a broad Ni $2p_{3/2}$ peak with the shoulder feature marked by the dashed line at 852.7 eV, which corresponds to the $2p_{3/2}$ electron binding energy of metallic Ni. The rest of the broad Ni $2p_{3/2}$ peak at the higher binding energy side indicates the presence of an oxidized surface layer, which was formed during the shelf period waiting for the XPS analysis. For the as-prepared karst-Ni thin film and a karst-Ni thin film after 10 cycles of the CV scan (−0.9 to 0.2 V vs. SCE) in the aqueous solution of 1 M KOH + 1 M CH_3OH, the Ni $2p_{3/2}$ signal is primarily emitted from oxidized Ni species with little contribution from the metallic phase. As discussed later in more detail, the oxidized surface layer comprise various oxidized Ni species, such as NiO, $Ni(OH)_2$ and NiOOH. Combined with the XRD result, the XPS analysis suggests that the karst-Ni nanostructures has a metallic core, which is overlaid by a Ni oxide layer with a thickness larger than the escape depth of the Ni $2p_{3/2}$ photoelectron (~5 nm). The metallic Ni core is desirable for fast electrochemical kinetics for MOR in the alkaline solution because it has a good electrical conductivity.

3.2. Electrochemical measurements

Fig. 5 shows cyclic voltammograms (CV) of methanol electro-oxidation in the aqueous solution of 1 M CH_3OH and 1 M KOH for the Pt/karst-Ni, the Pt/Ni and the blanket-Pt electrodes. The CVs were taken over the range between −0.9 and +0.2 V at a scan rate of 20 mV s^{-1}. Because methanol oxidation electrocatalyzed by Ni in alkaline solutions occurs in a higher potential range (0.36–0.45 V vs. SCE) [22], the anodic peak in the CV curve must represent the contribution entirely from the MOR electrocatalyzed by Pt. The Pt/karst-Ni electrode exhibits a very good electrocatalytic activity toward MOR in the alkaline solution as shown by the much higher anodic peak maximum in the forward scan compared with the other two electrodes. The large forward anodic current of the Pt/karst-Ni electrode can be ascribed to its large electrochemical surface active area (ESA). As determined from the CO stripping CV measurement in the 1 M KOH solution (discussed later in Fig. 6), the Pt/karst-Ni, the Pt/Ni and the blanket-Pt electrodes have an ESA of 511.2, 258.9 and 75.8 m^2/g, respectively, assuming an oxidation charge of 0.484 mC for a monolayer of CO molecules adsorbed on a smooth Pt surface [12]. The peak potential of MOR for the Pt/karst-Ni electrode is −0.31 V vs. SCE with the onset potential at −0.54 V, which is herein defined as the MOR potential at which the current density reaches 10% of the peak maximum. For the

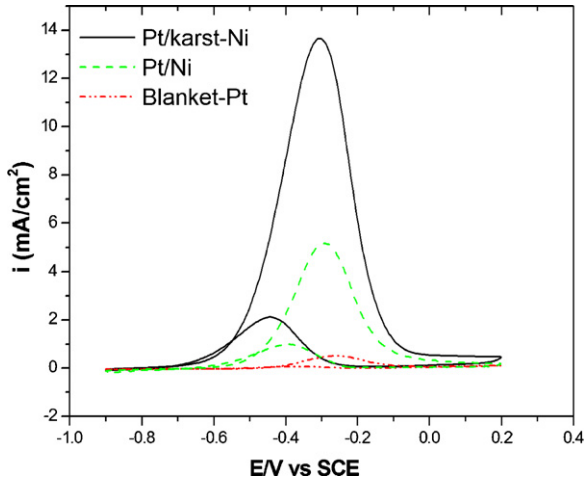

Fig. 5. Cyclic voltammograms of methanol electro-oxidation for the Pt/karst-Ni, the Pt/Ni and the blanket-Pt electrodes in the aqueous solution of 1 M CH_3OH + 1 M KOH. The scan rate was 20 mV s^{-1}. The current density is normalized to the sample surface area.

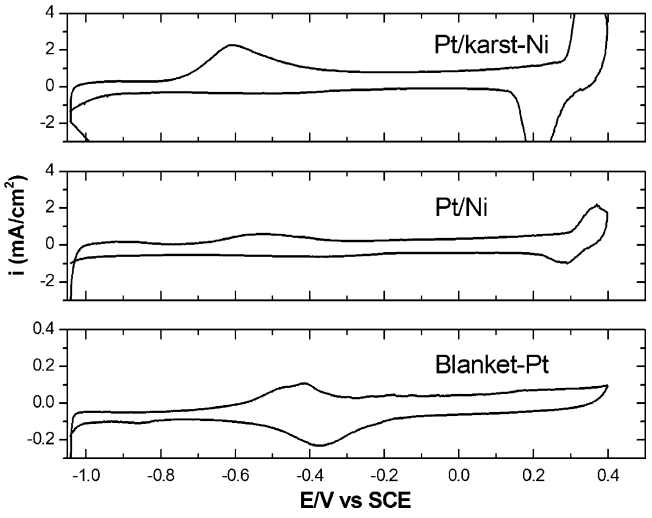

Fig. 6. CO stripping cyclic voltammograms of the Pt/karst-Ni, the Pt/Ni and the blanket-Pt electrodes in the CO saturated 1 M KOH solution. The scan rate was 20 mV s^{-1}. The current density is normalized to the sample surface area.

Pt/Ni electrode, the MOR peak potential and the onset potential are situated at −0.29 V and −0.49 V vs. SCE, respectively. The blanket-Pt electrode has the MOR peak potential (−0.25 V) and the onset potential (−0.45 V) less negative than the two Ni-supported electrodes, suggesting that the Ni supports can improve the electrocatalytic activity.

In addition to a large ESA, efficient removal of carbonaceous intermediates or residuals from the Pt catalyst surface during MOR is crucial to the electrocatalytic performance of an electrode. In CV measurements for methanol electro-oxidation in alkaline electrolytes, the anodic peaks in the forward scan is associated with chemisorption of methanol molecules and oxidation of intermediate organic species, and the anodic peak in the reverse scan is due to oxidation of weakly bonded CHO species, which are incompletely oxidized intermediates in the forward scan [17]. The ratio of the forward anodic current (I_f) to the reverse anodic current (I_b), I_f/I_b, is generally used as a simple index to signify the ability of the Pt catalyst to resist CO poisoning during MOR [7,12,27]. A small I_f/I_b value indicates that the methanol electro-oxidation reaction has a poor kinetics, leaving excessive carbonaceous adspecies on the Pt catalyst surface. From Fig. 5, the I_f/I_b ratios of the Pt/karst-Ni, the Pt/Ni and the blanket-Pt electrodes are 6.25, 5.67 and 4.92, respectively, indicating that electrodes using Ni as the Pt catalyst support have better CO tolerance in the KOH electrolyte than the blanket-Pt electrode. The CO stripping CV measurement discussed below provides direct evidences of better CO tolerance of the Ni supported Pt catalyst in the alkaline solution.

The CO-stripping cyclic voltammograms of the three electrodes are shown in Fig. 6. For both the Ni supported Pt electrodes, a single broad peak is observed within the range between −0.8 and −0.1 V vs. SCE, while the blanket-Pt electrode has a doublet peak feature. In an acidic solution, CO adspecies on Pt usually exhibit two electro-oxidation peaks in CO stripping CVs [28–30], and the observation of the two potential peaks is ascribed to CO oxidation occurring on different lattice planes of the Pt electrocatalyst [28]. The doublet peak feature observed in the KOH solution may result from CO electro-oxidation at different lattice sites on the polycrystalline Pt thin film as well. The absence of the doublet peak feature for the two Ni-supported electrodes are likely due to that the electrodeposited Pt particles do not have a preferential distribution in the orientation planes that yield the characteristic doublet feature for CO electro-oxidation. The onset potential and the anodic peak potential are listed in pair for the Pt/karst-Ni, the Pt/Ni and the blanket-Pt electrodes, respectively, as follows: (−0.75 V, −0.62 V), (−0.72 V, −0.52 V) and (−0.69, −0.42), where in the parenthesis the first value is the onset potential. The lower CO stripping onset potential indicates that the Pt/karst-Ni electrode has a smaller overpotential for the CO electro-oxidation. Combined with the high ESA, the lower onset and peak potentials of CO electro-oxidation make the Pt/karst-Ni electrode much more electrocatalytically active toward MOR in the alkaline solution than the other two electrodes.

The improvement in the electro-oxidation activity of CO adspecies is generally ascribed to the bi-functional mechanism involved in the CO oxidation reaction and the electronic effect (ligand effect) due to charge transfer between the catalyst and the support [31,32]. In the bi-functional mechanism model, oxygen containing adspecies, such as hydroxyl surface groups, can oxidize CO adspecies on the Pt catalyst, thereby avoiding CO poisoning. The CO electro-oxidation reaction via the bi-functional mechanism can be expressed by the following equation.

$$CO_{Pt} + 2OH^-{}_M \rightarrow CO_2(g) + H_2O + 2e^-, \quad (1)$$

where the subscript M represents Pt atoms or hydroxylated sites (e.g. Ni-OH) immediately adjacent to a CO-bonded Pt site. Chemical reaction processes on a surface are generally described by either the Langmuir–Hinshelwood (L–H) mechanism or the Eley–Rideal (E–R) mechanism. For methanol electro-oxidation in acidic electrolytes, the bifunctional mechanism can be best understood by the L–H mechanism, in which adsorbed reactants migrate on the surface and reactions take place by collision between adspecies. The CO electro-oxidation reaction via the L–H mechanism requires that OH adspecies be present on the Pt catalyst surface. Because of the deficiency in OH^- ions in an acidic solution, OH adspecies on a Pt catalyst particle are primarily produced by dissociative adsorption of water molecules or OH spillover from neighboring hydroxylated sites. The ease of the CO oxidation reaction via the L–H mechanism greatly depends on adsorption properties of CO and OH adspecies, such as the (CO)–Pt bond strength and the surface diffusivity of CO and OH adspecies. Opposite to acidic solutions, alkaline electrolytes contain abundant OH^- ions, and thus the E–R mechanism should also be considered an important reaction pathway leading to the CO electro-oxidation and removal. In an E–R surface reaction, the reaction product is formed by direct collision of a reactant species from the solution phase with a reactant adspecies. According to the E–R mechanism model, CO adspecies on the Pt catalyst can be readily oxidized by OH^- ions diffusing from the bulk alkaline electrolyte. Because all the three electrodes of this study are immersed in the KOH solution of the same chemical ingredients, the collision rate per unit area of OH^- ions with CO adspecies on the three electrode must be the same. Under such condition, the E–R mechanism should be more prevailing on the electrode with CO adsorption structures allowing more effective CO oxidation and easier (CO)–Pt bond breaking. From the above discussion, for both the E–R and the L–H mechanisms, the electrochemical activity of the CO oxidation reaction is closely related to adsorption properties of the CO adspecies. Because CO adsorption properties are governed by surface properties of the Pt catalyst, which can be modified by the Ni support, the electronic interaction between the Pt catalyst and the Ni support can greatly influence the electrochemical activity of CO oxidation on the Ni-supported electrodes of this study. According to XPS analysis, the Pt/karst-Ni and the Pt/Ni electrodes have a large negative shift in the Pt $4f_{7/2}$ binding energy, indicating that charge transfer occurs between the Pt catalyst and the Ni support.

The Pt(4f) XPS spectrum of the Pt/karst-Ni thin film shown in Fig. 7 exhibits a doublet peak with the Pt $4f_{7/2}$ peak maximum at 70.7 eV, which negatively shifts from that of the blanket Pt thin

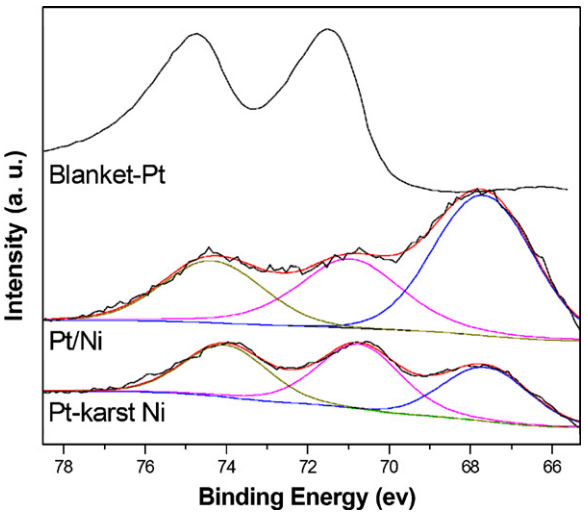

Fig. 7. The Pt 4f XPS spectra of the Pt/karst-Ni, the Pt/Ni and the blanket-Pt electrodes. In the spectra of the two Ni-supported electrodes, the peak situated around 67.6 eV is due to the Ni 3p signal emitted from the Ni support. Curve fitting was carried out so that the Pt $4f_{7/2}$ binding energy for the two Ni-supported electrodes could be more accurately determined.

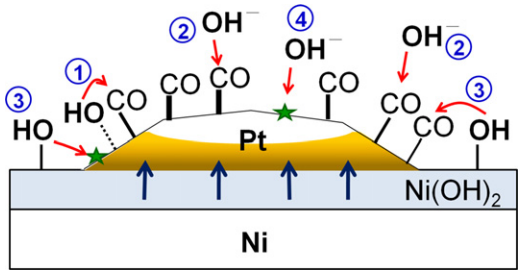

Fig. 8. Schematic illustration of the synergistic effect of the bifunctional mechanism and the electronic effect for CO electro-oxidation on Pt nanoparticles adhered to the Ni support. The arrows represent negative charge transfer from the $Ni(OH)_2$ surface layer to the Pt nanoparticle. The gradually shaded color indicates the degree of the induced electronic modification on the Pt nanoparticle as a result of the charge transfer. The thickness of the lines connecting CO adspecies with Pt nanoparticle represents the magnitude of the bond strength, which depends on the degree of the electronic modification and exposed surface lattice planes of the Pt nanoparticle. The reactions numbered by 1 and 2 denote CO oxidation by an OH adspecies via the L–H mechanism and by an OH^- ion from the electrolyte via the E–R mechanism, respectively. The processes numbered by 3 represent that an OH surface group on the $Ni(OH)_2$ surface layer reacts with an neighboring CO adspecies on the Pt nanoparticle, or migrates to a free surface site (labeled by the star symbol) on the nanoparticle. The OH^- ion numbered by 4 denotes the diffusion of the OH^- ion toward a free surface site, which can be created by the removal of an oxidized CO adspecies.

film by ~0.7 eV. The negative binding energy shift of the Pt 4f doublet peak can be ascribed to either the nanometer-size effect of Pt nanoparticles or charge transfer between Pt nanoparticles and the Ni support, or a combination of the both effects. It has been widely reported that the binding energy of core level electrons of metal nanoparticles shifts from that of the bulk counterparts as a function of the particle size [33–35]. The binding energy shift generally increases with decreasing the size of metal nanoparticles; and the size effect on the energy shift becomes insignificant when the particle size is larger than 3 nm [33]. Because Pt nanoparticles on the Pt/karst-Ni electrode have a particle size around 5 nm, the large negative shift (−0.7 eV) in the Pt $4f_{7/2}$ binding energy suggests that negative charge transfer from the karst-Ni support to Pt nanoparticles has occurred. A theoretical study showed that, upon adsorption on the NiO(1 0 0) surface, Pt atoms sit on the oxygen-top site and form strong chemical bonds with the surface as a result of a change in the electronic configuration of Pt atoms [36]. It is likely that Pt atoms adsorbed on nickel hydroxides are also subject to a strong electronic modification. Surface atoms of a smaller Pt nanoparticle should experience a larger electronic modification because of their close proximity to the interface between the nanoparticle and the Ni support, at where the charge transfer takes place. For the Pt/Ni electrode, the curve-fitted Pt $4f_{7/2}$ peak has the maximum at 71.0 eV and has a slightly larger full-width-at-half-maximum (FWHM) than the Pt/karst-Ni electrode. The less negative Pt 4f energy shift and the larger FWHM indicate that Pt particles on the Pt/Ni electrode have a smaller electronic modification with a wider distribution of the modification strength. This is because the Pt particles on the Pt/Ni electrode have a wide size distribution ranging from a few to a few hundred nanometers, and, as a result, surface atoms clearly experiencing the electronic modification are far fewer than atoms lacking the modification. Fig. 8 schematically illustrates the progressive decrease in the electronic modification as a function of the distance from the interface between a Pt nanoparticle and the hydroxylated Ni support. The colored area indicates the region affected by the charge transfer between the Pt nanoparticle and the Ni support, and the gradually shaded color represents the degree of the induced electronic modification. A smaller nanoparticle is apparently has a larger portion of surface atoms that are subject to the electronic modification. Because of the greater electronic modification of Pt nanoparticles, the Pt/karst-Ni electrode must exhibit an electrocatalytic activity distinct from the Pt/Ni and the blanket-Pt electrodes. The better CO electro-oxidation performance for the Pt/karst-Ni electrode, as shown in Fig. 6, suggests that the electronic modification due to the charge transfer results in a (CO)–Pt adsorption structure that enhances the CO electro-oxidation activity in the alkaline solution. The Pt/Ni electrode also benefits from the electronic modification for better CO tolerance although the improvement is less significant than the Pt/karst-Ni electrode.

In a study of the mechanism of CO oxidation in NaOH solutions, Spendelow et al. found that CO electro-oxidation on the Pt(1 1 1) surface was primarily via the L–H mechanism [37]. In such case, OH adspecies must be present on the Pt catalyst surface so that the CO oxidation reaction can proceed, as shown by reaction (1) in Fig. 8. A previous study has shown that OH adsorption on the Pt(1 1 1) surface in alkaline solutions occurs in the potential range between 0.65 and 0.85 V vs. RHE (equivalent to −0.36 to −0.16 V vs. SCE) [38]. The potential range for OH adsorption on the Pt(1 1 1) surface is much less negative than the measured potential range (−0.8 to −0.4 V vs. SCE) for the CO electro-oxidation reaction occurring on the Pt/karst-Ni electrode. Although Pt nanoparticles on the Pt/karst-Ni electrode must comprise various surface lattice planes and defects, on which OH adsorption may take place at different potentials, the very negative CO stripping peak potential (~−0.6 V) suggests that OH adspecies produced on Pt nanoparticles during the CV scan are unimportant to the CO electro-oxidation reaction occurring on the Ni-supported electrode. Therefore, to facilitate CO electro-oxidation at the low potential region, OH spillover from the Ni support to Pt nanoparticles becomes a likely channel to supply OH adspecies needed for the CO electro-oxidation reaction via the L–H mechanism. Ni is readily oxidized in alkaline solutions, forming various hydroxides on the substrate surface [23,39]. According to the Ni 2p XPS spectrum shown in Fig. 9, the surface of a karst-Ni thin film (before Pt electrodeposition) is rich in hydroxylated species after a 10-cycle CV scan in the aqueous solution of 1 M KOH + 1 M CH_3OH. The spectrum was curve-fitted assuming a Gaussian–Lorentzian peak shape and the binding energies for the fitted peaks were determined by referring to literature data [40–43]. The XPS analysis shows that $Ni(OH)_2$ is the most abundant chemical phase on the surface of the Ni support, and a significant amount of NiOOH is also present on the surface. Nickel oxidation on a Ni electrode in alkaline media can be expressed by the following

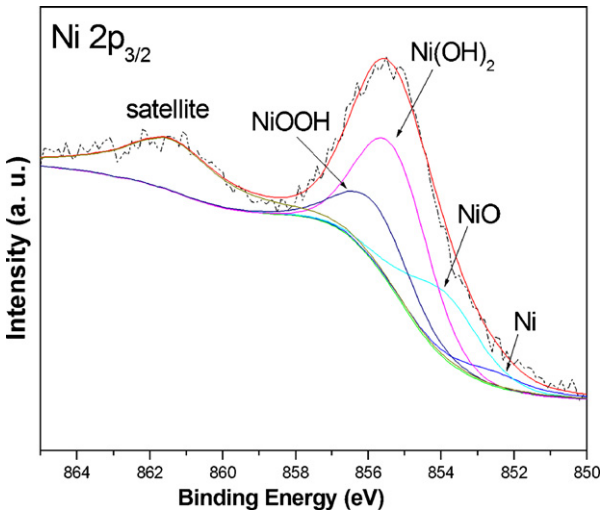

Fig. 9. Ni $2p_{3/2}$ XPS spectrum of a karst-Ni thin film after a 10-cycle CV scan in the aqueous solution of 1 M CH_3OH + 1 M KOH. Curve fitting was carried out to resolve the component peaks of metallic Ni, NiO, $Ni(OH)_2$ and NiOOH.

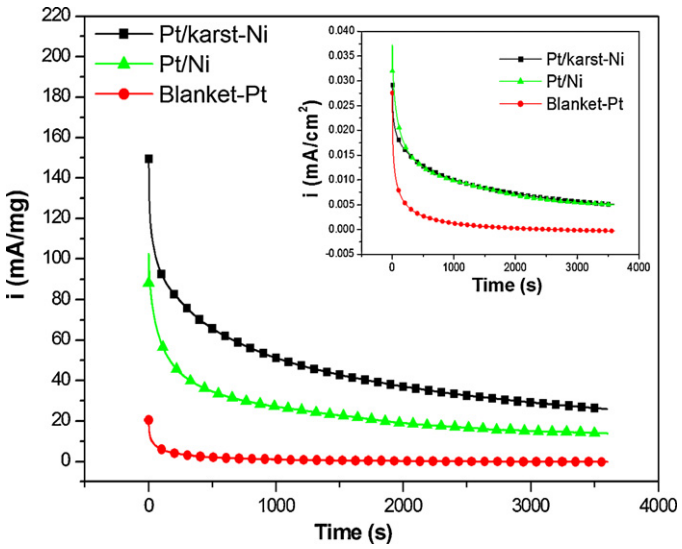

Fig. 10. Chronoamperometry curves of the Pt/karst-Ni, the Pt/Ni and the blanket-Pt electrodes in the aqueous solution of 1 M CH_3OH + 1 M KOH at room temperature for 1 h. The oxidation potential was kept at −0.3 vs. SCE. The inset shows the same chronoamperometric results but the y-axis label "mass activity" is replaced by the current density normalized to the electrochemical surface area.

reactions: [23]

$$Ni + 2OH^- \rightleftharpoons Ni(OH)_2 + 2e^-, \quad (2)$$

$$Ni(OH)_2 + OH^- \rightleftharpoons NiOOH + H_2O + e^-. \quad (3)$$

$Ni(OH)_2$ is formed on the Ni surface in the potential range between −1.1 and −0.6 V vs. SCE, and the transformation of α-$Ni(OH)_2$ to β-$Ni(OH)_2$ occurs in the range from −0.6 to 0.3 V vs. SCE [39]. Further oxidation of $Ni(OH)_2$ to NiOOH proceeds at a higher potential (~0.4 V vs. SCE) [39]. Because CO oxidation on the three electrodes of this study occurs at a potential much smaller than the formation potential of the NiOOH phase, OH adspecies involved in the CO electro-oxidation reaction via the L–H mechanism must be mainly provided by the $Ni(OH)_2$ phase. As discussed above, a Pt nanoparticle has a high CO electro-oxidation activity in the perimeter because of the strong electronic interaction between Pt atoms in the perimeter and the Ni support. OH surface groups stemming from the $Ni(OH)_2$ phase and surrounding a Pt nanoparticle can either migrate to empty surface sites in the perimeter of the Pt nanoparticle or react directly with neighboring CO adspecies on the Pt nanoparticle (as shown by reaction (3) in Fig. 8). Therefore, CO electro-oxidation via the L–H mechanism should be more pronounced in the peripheral region of a Pt nanoparticle than in the inner area. New empty surface sites are created in the perimeter of the Pt nanoparticle after oxidized CO adspecies are removed, and can be reoccupied by CO or OH adspecies migrating on the nanoparticle, allowing progressive CO oxidation through the particle surface via the L–H mechanism. The L–H model scenario is more applicable to Pt nanoparticles of smaller size. On a smaller particle, OH and CO adspecies can migrate over the particle in a shorter time, resulting in a higher collision rate between CO and OH adspecies, and thus a more efficient CO electro-oxidation reaction.

Although Spendelow et al. [37] has proposed that CO electro-oxidation via the L–H mechanism predominates on the Pt(1 1 1) surface in alkaline electrolyte, we cannot rule out the participation of the E–R mechanism in the CO electro-oxidation reaction on the Ni-supported electrodes. Because Pt nanoparticles on the electrodes must comprise defects and surface planes other than the Pt(1 1 1) plane, it is likely that these surface sites may provide an adsorption environment for CO adspecies allowing oxidation by OH anions from the alkaline electrolyte via the E–R mechanism. If the E–R reaction takes place, like the CO oxidation reaction via the L–H mechanism, the catalyst particle size can influence the eletroactivity of the CO oxidation reaction via the E–R mechanism as well. When CO adspecies have an adsorption structure kinetically favoring the CO electro-oxidation reaction via the E–R mechanism, collision of the CO adspecies with OH^- ions diffusing from the bulk electrolyte (as shown by reaction (2) in Fig. 8) will lead to a high electro-oxidation activity. If the electronic modification results in a CO adsorption structure that can enhance CO electro-oxidation via the E–R mechanism, a smaller Pt particle will have a higher electrocatalytic activity toward CO electro-oxidation than a larger one.

Fig. 10 shows chronoamperograms of the Pt/karst-Ni, the Pt/Ni and the blanket-Pt electrodes at the oxidation potential of −0.3 V vs. SCE in the aqueous solution of 1 M CH_3OH + 1 M KOH. All the three electrodes demonstrate a gradual decrease in the mass activity with the polarization time. In addition to the possible carbonaceous residue left on the Pt catalyst due to incomplete methanol electrooxidation, Pt catalyst loss and/or agglomeration may take place and thus reduce the ESA. Moreover, the reaction between the alkaline electrolyte and CO_2, which is the product of CO electrooxidation, can produce carbonates [1,9,44]. Formation of insoluble carbonates may consume the electrolyte and/or block active sites on the anode, thereby degrading the electrocatalytic performance of the electrode. For the blanket-Pt electrode, the mass activity rapidly drops to ~3.1 mA/mg within the first 300 s and becomes nearly zero mA/mg after one hour of the test. For the Pt/Ni electrode, the drop of the mass activity is less severe compared with the blanket-Pt electrode, and the mass activity decreases to ~13.7 mA/mg after one hour of the methanol electro-oxidation. On the other hand, the Pt/karst-Ni electrode maintains a high mass activity through the electrochemical test and has a mass activity of ~27.1 mA/mg at the end of the 1-hr measurement. The inset of Fig. 10 presents the same chronoamperometric results but with the labeled current density normalized to the electrochemical surface area. The inset shows that the two Ni-based electrodes have similar chronoamperometric properties. The better electrocatalytic performance of the two Ni-based electrodes for MOR in the alkaline solution can be ascribed to better CO tolerance, which is a result of the synergistic effect of the bifunctional mechanism and the strong electronic interaction between the Pt catalyst and the Ni support. The steady and high mass activity of the Pt/karst-Ni

electrode also infers that Pt nanoparticles pulse-electrodeposited on the rugged karst-Ni support are electrochemically stable in the alkaline solution. The Pt/Ni-karst electrode has a higher mass activity than the Pt/Ni electrode, and is thus a better electrode for methanol oxidation in respect to the utilization of the precious Pt catalyst.

4. Conclusions

The study prepared rugged Ni thin films on the Si substrate by HNO_3 wet etch, and the etched Ni thin films were used as Pt catalyst supports for the study on electrocatalytic MOR in the aqueous KOH solution. Pt nanoparticles of ~5 nm in size were successfully pulse-electrodeposited on the Ni support. The rugged Ni thin film has a karst-like surface morphology, and comprises irregular nanostructures featuring a metallic Ni core capped by Ni oxides. XPS analysis shows that $Ni(OH)_2$ is formed on the Ni support during the potential scan in the alkaline solution. The hydroxide may enhance CO tolerance of the Pt catalyst via the bi-functional mechanism and thus improve the electrocatalytic activity toward MOR. The L–H and the E–R mechanisms are used to elucidate the role of OH surface groups on the Ni support and OH^- ions in the KOH solution, respectively, in the enhancement of CO tolerance in the alkaline electrolyte. The negative shift in the Pt(4f) binding energies suggests that negative charge transfer takes place from the Ni support to the Pt catalyst. The electronic interaction may modify adsorption properties of CO adspecies on the Pt catalyst, and the modification on a Pt nanoparticle allows easy CO electro-oxidation by OH species surrounding the nanoparticles, either from the Ni support or from the alkaline solution. The synergistic effect of the bifunctional mechanism and the electronic interaction enhance CO tolerance of Pt nanoparticles, and thus the electrocatalytic activity toward MOR in the KOH solution. Because of the large electrochemical area and the nanometer-size of Pt particles, the Pt/karst-Ni electrode exhibits better electrocatalytic performance for MOR in the alkaline solution than the Pt/Ni and the blanket-Pt electrodes.

Acknowledgments

This work was supported by the National Science Council of R.O.C., under Contract No. NSC97-2221-E-009-016-MY3. The technical support from National Nano Device Laboratories is also gratefully acknowledged.

References

[1] L. Carrette, K.A. Friedrich, U. Stimming, Fuel Cells 1 (2001) 5–39.
[2] E. Antolini, J.R.C. Salgado, E.R. Gonzalez, Appl. Catal. B 63 (2006) 137–149.
[3] M.P. Hogarth, G.A. Hards, Platinum Met. Rev. 40 (1996) 150–159.
[4] K.-W. Park, J.-H. Choi, B.-K. Kwon, S.-A. Lee, Y.-E. Sung, H.-Y. Ha, S.-A. Hong, H. Kim, A. Wieckowski, J. Phys. Chem. B 106 (2002) 1869–1877.
[5] J.S. Spendelow, G.Q. Lu, P.J.A. Kenis, A. Wieckowski, J. Electroanal. Chem. 568 (2004) 215–224.
[6] A.V. Tripkovic, K.D. Popovic, B.N. Grgur, B. Blizanac, P.N. Ross, N.M. Markovic, Electrochim. Acta 47 (2002) 3707–3714.
[7] Z. Liu, X.Y. Ling, X. Su, J.Y. Lee, L.M. Gan, J. Power Sources 149 (2005) 1–7.
[8] E.E. Switzer, T.S. Olson, A.K. Datye, P. Atanassov, M.R. Hibbs, C.J. Cornelius, Electrochim. Acta 54 (2009) 989–995.
[9] J. Bagchi, S.K. Bhattacharya, J. Power Sources 163 (2007) 661–670.
[10] F.C. Simões, D.M. dos Anjos, F. Vigier, J.M. Léger, F. Hahn, C. Coutanceau, E.R. Gonzalez, G. Tremiliosi-Filho, A.R. de Andrade, P. Olivi, K.B. Kokoh, J. Power Sources 167 (2007) 1–10.
[11] S.T. Nguyen, H.M. Law, H.T. Nguyen, N. Kristian, S. Wang, S.H. Chan, X. Wang, Appl. Catal. B 91 (2009) 507–515.
[12] C.-S. Chen, F.-M. Pan, Appl. Catal. B 91 (2009) 663–669.
[13] C. Xu, Z. Tian, P. Shen, S.P. Jiang, Electrochim. Acta 53 (2008) 2610–2618.
[14] L.X. Yang, C. Bock, B. MacDougall, J. Park, J. Appl. Electrochem. 34 (2004) 427–438.
[15] Y.-J. Gu, W.-T. Wong, J. Electrochem. Soc. 153 (2006) A1714–A1718.
[16] M.S. Saha, R. Li, M. Cai, X. Sun, Electrochem. Solid-State Lett. 10 (2007) B130–B133.
[17] J. Prabhuram, R. Manoharan, J. Power Sources 74 (1998) 54–61.
[18] N.M. Markovic, C.A. Lucas, A. Rodes, V. Stamenkovic, P.N. Ross, Surf. Sci. 499 (2002) L149–L158.
[19] R.S. Ferreira Jr., V.R. Oliveira, R.G.C.S. Reis, G. Maia, G.A. Camara, J. Power Sources 185 (2008) 853–856.
[20] G.F. McLean, T. Niet, S. Prince-Richard, N. Djilali, Int. J. Hydrogen Energy 27 (2002) 507–526.
[21] K. Scott, E. Yu, G. Vlachogiannopoulos, M. Shivare, N. Duteanu, J. Power Sources 175 (2008) 452–457.
[22] A. Kowal, S.N. Port, R.J. Nichols, Catal. Today 38 (1997) 483–492.
[23] M.A. Abdel Rahim, R.M. Abdel Hameed, M.W. Khalil, J. Power Sources 134 (2004) 160–169.
[24] E. Herrero, K. Franaszczuk, A. Wieckowski, J. Phys. Chem. 98 (1994) 5074–5083.
[25] Y. Wang, T.S. Nguyen, X. Liu, X. Wang, J. Power Sources 195 (2010) 2619–2622.
[26] J.M. Léger, S. Rousseau, C. Coutanceau, F. Hahn, C. Lamy, Electrochim. Acta 50 (2005) 5118–5125.
[27] M.A. Scibioh, S.-K. Kim, E.A. Cho, T.-H. Lim, S.-A. Hong, H.Y. Ha, Appl. Catal. B 84 (2008) 773–782.
[28] U. Koponen, T. Peltonen, M. Bergelin, T. Mennola, M. Valkiainen, J. Kaskimies, M. Wasberg, J. Power Sources 86 (2000) 261–268.
[29] B.E. Hayden, A.J. Murray, R. Parsons, D.J. Pegg, J. Electroanal. Chem. 409 (1996) 51–63.
[30] M. Bergelin, J.M. Feliu, M. Wasberg, Electrochim. Acta 44 (1998) 1069–1075.
[31] J. Croy, S. Mostafa, J. Liu, Y. Sohn, H. Heinrich, B. Cuenya, Catal. Lett. 119 (2007) 209–216.
[32] J.N. Tiwari, F.-M. Pan, T.-M. Chen, R.N. Tiwari, K.-L. Lin, J. Power Sources 195 (2010) 729–735.
[33] S. Garbarino, A. Pereira, C. Hamel, E. Irissou, M. Chaker, D. Guay, J. Phys. Chem. C 114 (2010) 2980–2988.
[34] A. Howard, D.N.S. Clark, C.E.J. Mitchell, R.G. Egdell, V.R. Dhanak, Surf. Sci. 518 (2002) 210.
[35] P. Marcus, C. Hinnen, Surf. Sci. 392 (1997) 134–142.
[36] F. Cinquini, L. Giordano, G. Pacchioni, Theor. Chem. Acc. 120 (2008) 575–582.
[37] J.S. Spendelow, J.D. Goodpaster, P.J.A. Kenis, A. Wieckowski, J. Phys. Chem. B 110 (2006) 9545–9555.
[38] A.V. Tripković, K.D. Popović, J.D. Momčilović, D.M. Dražić, J. Electroanal. Chem. 418 (1996) 9–20.
[39] M. Vuković, J. Appl. Electrochem. 24 (1994) 878–882.
[40] H. Li, H. Li, W.-L. Dai, W. Wang, Z. Fang, J.-F. Deng, Appl. Surf. Sci. 152 (1999) 25–34.
[41] G.B. Hoflund, W.S. Epling, Chem. Mater. 10 (1998) 50–58.
[42] N.S. McIntyre, M.G. Cook, Anal. Chem. 47 (1975) 2208–2213.
[43] A.P. Grosvenor, M.C. Biesinger, R.S.C. Smart, N.S. McIntyre, Surf. Sci. 600 (2006) 1771–1779.
[44] A. Verma, S. Basu, J. Power Sources 174 (2007) 180.